Tensors - 1

Tensors

Used in engineering sciences & physics

In the context of solid mechanics:

- stresses & strains
- Anisotropic materials (most materials are)

  properties are different in different directions

- Moments of inertia
- CAD – rotations, stretching of figures

Physical quantities

- scalars (no direction, one number)
  - temperature
  - energy
- vectors (magnitude + direction)
  - force
  - velocity

  3 numbers

tensors — 9 quantities

- strain
- stress
- anisotropic conductivity
- inertia tensor $\underline{I}$

Notation : tensors underlined (as well as vectors) to distinguish them from scalars

Conductivity (thermal, or electric)

isotropic material: $\underset{\sim}{q} = k \underset{\sim}{\nabla T}$

the two vectors are parallel

Anisotropic material:

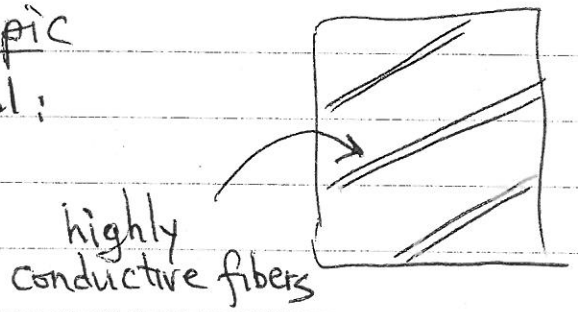

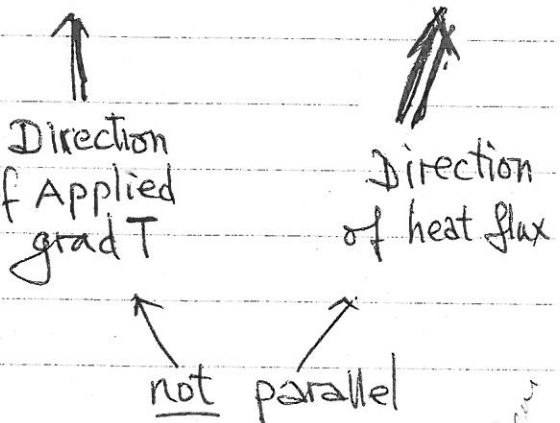

Linear conduction law (Fourier, or Ohm)

q_x, q_y, q_z — each is a linear combination of $\frac{\partial T}{\partial x}$, $\frac{\partial T}{\partial y}$, $\frac{\partial T}{\partial z}$

$\Rightarrow$ 9 quantities

(in contrast with only one, k, in case of isotropy)

Fluid filtration (through porous/microcracked material)

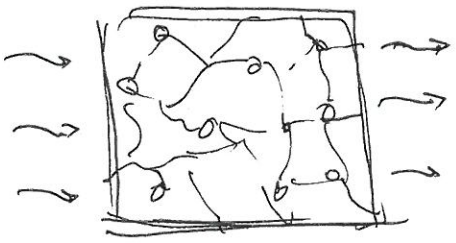

Driven by fluid pressure gradient ∇p

Fluid flux vector $\underset{\sim}{q}$: defined as : volume of fluid passing across surface element ΔA

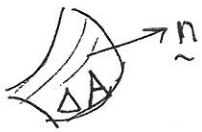

$= \underset{\sim}{q} \cdot \underset{\sim}{n} \, \Delta A$

Isotropic permeability:

$$\underset{\sim}{q} = -\frac{k}{\mu} \nabla p$$

(Darcy's law)

k – permeability coeff determined by microgeometry of ~~porous~~ space

μ – fluid viscosity

$\underset{\sim}{q}$ is in the direction of ∇p

Fluid filtration through anisotropic material (rocks, etc)

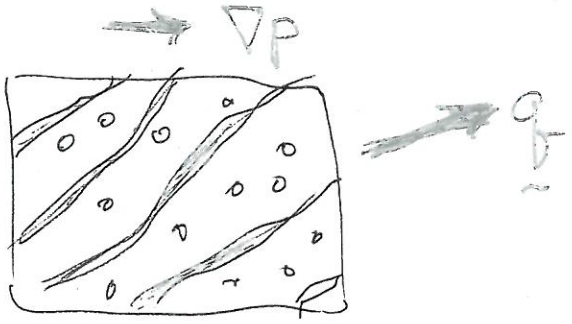

Darcy law: $\underset{\sim}{q}$ is linear f-n of ∇p

but not parallel to it

$$\begin{cases} q_x = -\frac{1}{\mu} k_{xx} \frac{\partial p}{\partial x} - \frac{1}{\mu} k_{xy} \frac{\partial p}{\partial y} - \frac{1}{\mu} k_{xz} \frac{\partial p}{\partial z} \\ q_y = \\ q_z = \end{cases}$$

3×3 matrix of permeability coefficients

Strain (deformation)

What makes deforming mat'l different from rigid body motion:

- mat'l lines stretch

This is a consequence of non-uniformity of displacem. field:

rigid body motion

How can we characterize this non-uniformity?

Displacem. vector $\underset{\sim}{u} = \underset{\sim}{u}(x, y, z)$ has 3 components, and

$$\left.\begin{aligned} u_x &= u_x(x,y,z) \\ u_y &= u_y(x,y,z) \\ u_z &= u_z(x,y,z) \end{aligned}\right\}$$

Non-uniformity of u_x:  $\frac{\partial u_x}{\partial x}, \frac{\partial u_x}{\partial y}, \frac{\partial u_x}{\partial z}$

Non-uniformity of u_y:  $\frac{\partial u_y}{\partial x}, \frac{\partial u_y}{\partial y}, \frac{\partial u_y}{\partial z}$

— — — — u_z — — — —

$\Rightarrow$ 9 quantities

CAD : - rotate
- stretch
- mirror - reflect
} transformations

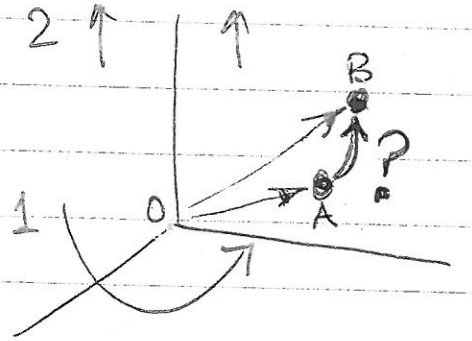

- where does point A go?

(how does position vector OA change, into OB?)

⇒ need to describe transformation of space (that incorporates rotation, stretch, done in sequence

Tensors are a necessity

for materials that are anisotropic

most of them are

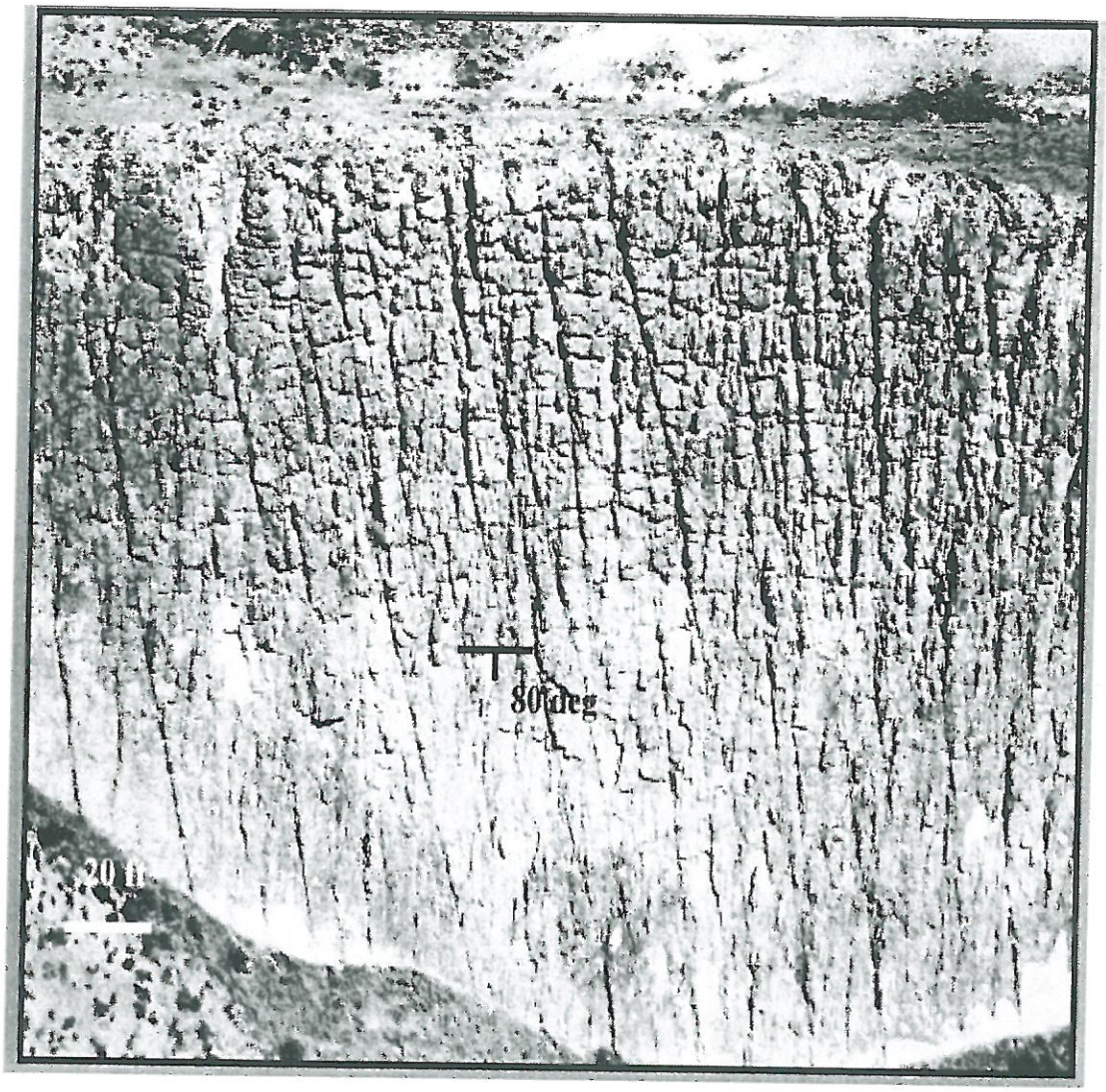

ROCK

Example of anisotropy : rock with parallel fractures

↓ tensors are needed

↓ causes anisotropy of elastic properties
Important for proper interpretation of acoustic data

GEOPHYSICS, VOL. 71, NO. 6 (NOVEMBER-DECEMBER 2006); P. W45–W58, 11 FIGS.
10.1190/1.2360212

Example, where tensors are needed

Effective elasticity of fractured rocks: A snapshot of the work in progress

Vladimir Grechka[1] and Mark Kachanov[2]

ABSTRACT

Exploration and development of naturally fractured reservoirs rely on understanding and interpretation of certain signatures associated with seismic waves propagating through cracked rocks. This understanding comes primarily from the effective media theories that predict an overall elastic behavior of a solid containing many inhomogeneities (cracks, in particular) whose sizes are too small to be "seen" individually by the waves. To model seismic responses of fractured formations, a geophysicist typically has a choice between the effective media schemes of Hudson and Schoenberg. While the two predictions usually deviate slightly for liquid-filled cracks, the differences are significant when the fractures are dry. Explaining the origin of these differences and selecting a more accurate scheme is the first goal of this tutorial. Our second, more challenging task, is to prove that simply adding the compliance contributions of cracks as if they were isolated and noninteracting remains sufficiently accurate even for fractures that grossly violate the basic theoretical assumption, of penny-shaped cracks. Real fractures have notoriously irregular shapes, might be partially closed, and often form interconnected networks. Yet, these details of fracture microgeometry turn out to be unimportant for the effective elasticity given a typical noise level in seismic data. No closed-form theory exists for irregular fracture shapes. However, take into account finite-element simulations on so-called digital rocks demonstrate which features of the crack geometry have to be taken into account because they influence propagation of long (compared to the size of fractures) seismic waves and which features can be ignored.

INTRODUCTION

Continuous depletion of conventional clastic hydrocarbon fields makes naturally fractured reservoirs an important target for the oil industry. Production of these reservoirs, whose matrix permeability often lies in the microdarcy range, is controlled by the networks of natural cracks that provide highly permeable conduits for fluid flow. Given the importance of fractures for production, such reservoir development is greatly aided by any information about the cracks obtained from seismic data. Although fractures in the subsurface usually come in all sizes, here we restrict our discussion to the cracks whose sizes are much smaller than the seismic wavelengths used in a particular application. Seismic waves cannot "see" such cracks individually. Instead, the measured wave signatures are governed by certain average characteristics of multiple fractures.

Analysis of these signatures reveals that a low-frequency seismic response of a fractured rock can be reproduced in a properly selected homogeneous solid. This fact justifies the use of the so-called effective media or homogenization theories that aim at replacing a microheterogeneous material with a homogeneous one that is equivalent to the former in the regime of static deformation. The overall properties of cracked solids are of obvious relevance to many materials science problems, and development of the effective media theories began there with a seminal paper of Eshelby (1957), which discusses a single ellipsoidal inclusion in an otherwise homogeneous elastic solid, and a paper of Bristow (1960) explicitly devoted to thin cracks. The first rock physics applications of the effective media theories are attributable to Walsh (1965a, b) for rocks with dry cracks and to O'Connell and Budiansky (1974) for cracks filled with a liquid. All the above mentioned and numerous other authors describe fractures as compliant inclusions in a relatively stiff unfractured matrix. While other possibilities have been exploited also (for instance, one can treat cracks as contacts of rough surfaces or as infinite thin soft layers with occasional asperities), this tutorial is exclusively devoted to the inclusion model of cracks as the most common.

It took longer for the exploration community to address these issues, and then papers by Hudson (1980) and Schoenberg (1980) appeared. Even though substantial progress in effective media theories has been made both in materials and earth sciences since 1980, today's typical geophysicist, examining seismic data acquired over a fractured reservoir, still chooses between the Hudson's theory and the linear slip theory of Schoenberg. Such a choice is not straightfor-

Manuscript received by the Editor March 9, 2006; revised manuscript received June 1, 2006; published online November 3, 2006.
[1]Shell International Exploration and Production, Inc., 3737 Bellaire Blvd., P.O. Box 481, Houston, Texas 77001. E-mail: vladimir.grechka@shell.com.
[2]Tufts University, Department of Mechanical Engineering, Medford, Massachusetts 02155. E-mail: mark.kachanov@tufts.edu.

$$2\Delta f = \boldsymbol{\tau}\cdot\boldsymbol{\tau}:\frac{1}{V}\sum_k (\mathbf{Znn}A)^{(k)}, \qquad (21)$$

thus, identifying the quantity $(1/V)\Sigma_k(\mathbf{Znn}A)^{(k)}$ as the proper crack-density tensor. It is symmetric and has the second rank; therefore, a material with any orientation distribution of scalar cracks is orthorhombic. Moreover, such orthorhombic media are rather special: Their anisotropy is elliptical and characterized by only four independent constants. We emphasize that

- The effective orthotropy is rooted in the (assumed) equalities $Z_N = Z_R = Z_T$.
- The crack-density tensor is derived from the elastic potential Δf.

The proportionality $\mathbf{Z} = Z\mathbf{I}$ takes place for circular cracks with an accuracy dependent on the background Poisson's ratio ν_b. Implications of such a proportionality, identified by Kachanov (1980, 1992, 1993), are discussed in the next section. Schoenberg and Sayers (1995) called the cracks satisfying equation 20 scalar. Grechka et al. (2006) numerically demonstrated that approximate equality $\mathbf{Z} = Z\mathbf{I}$ holds on average for multiple, noncircular cracks provided that their shape irregularities are random.

Dry circular cracks

For a circular dry crack that has radius a, the normal and shear compliances are not equal,

$$Z_N = \frac{16a(1-\nu_b^2)}{3\pi E_b} \quad \text{and} \quad Z_R = Z_T = \frac{Z_N}{1-\nu_b/2}; \qquad (22)$$

however, they are relatively close because the (usually positive) Poisson's ratio ν_b satisfies inequality $\nu_b \le 1/2$. The difference between Z_N and Z_T leads to the following form of the potential Δf (Kachanov, 1980):

$$\Delta f = \frac{16(1-\nu_b^2)}{3E_b(2-\nu_b)}[(\boldsymbol{\tau}\cdot\boldsymbol{\tau}):\boldsymbol{\alpha} + \boldsymbol{\tau}:\boldsymbol{\beta}:\boldsymbol{\tau}], \qquad (23)$$

where

$$\boldsymbol{\alpha} = \frac{1}{V}\sum_k (a^3\mathbf{nn})^{(k)} \qquad (24)$$

and

$$\boldsymbol{\beta} = -\frac{\nu_b}{2}\frac{1}{V}\sum_k (a^3\mathbf{nnnn})^{(k)}. \qquad (25)$$

Two tensors $\boldsymbol{\alpha}$ and $\boldsymbol{\beta}$ contain all information about the crack distribution over orientations and sizes relevant for the effective properties in the noninteraction approximation. The second-rank crack-density tensor $\boldsymbol{\alpha}$ can be viewed as a natural tensorial extension of the scalar crack density

$$e = \frac{1}{V}\sum_k (a^3)^{(k)} \equiv \mathrm{tr}\boldsymbol{\alpha} \qquad (26)$$

defined by Bristow (1960).

Remarkably, the crack widths or the aspect ratios θ do not enter equations 23–25, implying that the effective properties of solids with dry fractures are almost independent of θ (provided that $\theta \ll 1$). Consequently, the crack-related porosity has virtually no influence on the effective elasticity.

According to equations 23 and 25, dry, circular cracks become scalar (in the terminology of Schoenberg and Sayers, 1995) only when the background has zero Poisson's ratio ν_b. In reality, $\nu_b \neq 0$; however, the influence of $\boldsymbol{\beta}$-term in equation 23 is still relatively minor as a result of the multiplier $\nu_b/2$ (equation 25) that cannot be greater than one-fourth. Hence, neglecting this term and retaining $\boldsymbol{\alpha}$ as the sole crack-density parameter constitutes a reasonable approximation; computational studies of Grechka and Kachanov (2006a; 2006b) confirm its accuracy. Thus, we are back to the conclusion drawn for the (unrealistic) scalar fractures: A solid with arbitrarily oriented circular cracks is nearly orthorhombic. Moreover, one's ability to describe the effective elasticity in terms of just $\boldsymbol{\alpha}$ results in the following important properties of the crack-induced anisotropy:

- The overall influence of multiple, differently oriented dry fracture sets is indistinguishable from that of three orthogonal sets.
- The normals to these equivalent sets coincide with the principal directions of tensor $\boldsymbol{\alpha}$; the corresponding principal crack densities are the eigenvalues of $\boldsymbol{\alpha}$.
- The crack-induced orthotropy is elliptical. Furthermore, it is controlled by only four independent quantities [the combinations of E_b, ν_b, and three eigenvalues of $\boldsymbol{\alpha}$; see Kachanov (1980; 1993) for detail] rather than nine needed for general orthotropy. This feature was exploited by Grechka and Kachanov (2006a), who proposed a fracture-characterization technique capable of handling multiple sets of vertical cracks.

Differentiating Δf given by equation 23 with respect to $\boldsymbol{\tau}$ and using definitions 9, 16, and 17, we get an equivalent result in compliances (Kachanov, 1980; Sayers and Kachanov, 1995; Schoenberg and Sayers, 1995):

$$\Delta s_{ijlm} = \frac{8(1-\nu_b^2)}{3E_b(2-\nu_b)}(\alpha_{il}\delta_{jm} + \alpha_{im}\delta_{jl} + \alpha_{jl}\delta_{lm} + \alpha_{jm}\delta_{il} + 4\beta_{ijlm}), \quad (i,j,l,m = 1,2,3), \qquad (27)$$

where δ_{jm} is the Kronecker delta. Either ignoring tensor $\boldsymbol{\beta}$ in equation 27 or approximating its components β_{ijlm} with $-\nu_b(\alpha_{il}\delta_{jm} + \alpha_{im}\delta_{jl} + \alpha_{jl}\delta_{im} + \alpha_{jm}\delta_{il})/8$, we recover the effective elliptical orthotropy.

In summary, the theoretically predicted effective orthotropy of a simplified type for multiple sets of dry, penny-shaped fractures is subject to two assumptions:

1) The average over cracks equality of the normal and shear fracture compliances
2) The noninteraction approximation

We will test both assumptions numerically and show that their accuracy and range of applicability are sufficient for seismic needs.

Liquid-filled fractures

The influence of liquid infill on the overall compliance was first examined by O'Connell and Budiansky (1974) and Budiansky and O'Connell (1976) for cracks with (somewhat unrealistic for rocks)

Example: bone is anisotropic

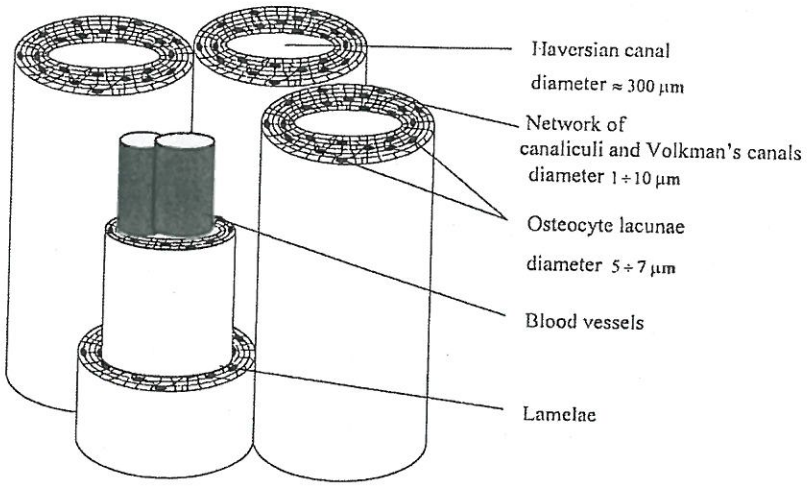

Fig. 1. Microstructure of the osteonal cortical bone according to Martin and Burr (1989) and Fung (1993). Canals and osteons are not to scale.

Table 2
Components H_{ijkl} for various pores (direction 3 is along the symmetry axis of the pore) and $\sum H_{ijkl}$ for the pore systems in bones (direction 3 is along the long axis of the bone). All the components are normalized to $E_0 V/V_{cav}$

	H_{1111}	H_{3333}	H_{1122}	H_{1133}	H_{1212}	H_{1313}
Single cylinder (empty)	2.82	1.00	− 0.82	− 0.30	3.64	2.60
Same (filled with soft material)	2.79	0.94	− 0.80	− 0.28	3.59	2.56
Single oblate spheroid	2.40	1.41	− 0.61	− 0.41	3.02	2.38
Same (filled with soft material)	2.38	1.40	− 0.59	− 0.39	2.97	2.36
	$\sum H_{1111}$	$\sum H_{3333}$	$\sum H_{1122}$	$\sum H_{1133}$	$\sum H_{1212}$	$\sum H_{1313}$
Haversian canals	2.82	1.00	− 0.82	− 0.30	3.64	2.60
Osteocyte lacunae	2.52	0.38	− 1.02	− 0.51	3.54	2.70
Canaliculi	2.66	0.46	− 1.05	− 0.56	3.71	3.12

osteocyte lacunae with the total surface area 5 mm^2/mm^3, about 10^6 canaliculi with the total surface area of 160 mm^2/mm^3 and about 20 Haversian canals with the total surface area of 3 mm^2/mm^3 (Martin and Burr, 1989). These numbers imply partial porosities for each of these types in the range 0.075–0.120. Since some researchers (Morris et al., 1982; Cowin, 1999) reported smaller porosities, we consider, in our analysis, a relatively wide range of porosities and examine the influence of porosity on the effective elastic moduli.

For the calculation of the effective moduli, we have to assume a certain value of the average aspect ratio of oblate lacunae. Different authors give somewhat different values of this ratio. We take this ratio to be $\frac{1}{2}$, i.e. $a_1 = a_2 = 2a_3$, according to the observations of Currey (1962). The symmetry axes of lacunae tend to lie in planes perpendicular to Haversian canals and do not appear to have any preferential orientations in these planes (Martin and Burr, 1989). Accordingly, we model the orientational distribution of lacunae by setting the symmetry axes to lie in the mentioned planes and to be randomly oriented in these planes.

We model the mineralized tissue (bone matrix) as the isotropic "background", thus ignoring the bone matrix anisotropy. There are several reasons for this simplification. First, as analysis of various pores in anisotropic matrix shows (Mauge and Kachanov, 1994), the impact of porous space on the overall response becomes dominant, as compared to the matrix anisotropy, at relatively moderate pore densities. Second, reasonably accurate experimental data on the full set of anisotropic constants of the bone matrix material are not presently available. Third, a sophisticated mathematical apparatus required for the three-dimensional analysis of anisotropic porous space in an anisotropic matrix is not presently available. Our results show that, in spite of this simplification, the anisotropic Young's and shear moduli are predicted quite well quantitatively, although a quantitative prediction of Poisson's ratios remains a problem.

To estimate constants E_0 and ν_0 of the bone matrix, we model it as a composite consisting of the collagen matrix reinforced by hydroxyapatite crystals. Young's moduli of hydroxyapatite and collagen are taken as $E_{HA} = 114.0$ GPa (Gilmore and Katz, 1982) and

ELSEVIER

Bone Vol. 25, No. 4
October 1999:481–486

Example where tensors are needed:

Constitutive Relationships of Fabric, Density, and Elastic Properties in Cancellous Bone Architecture

J. KABEL,[1] B. VAN RIETBERGEN,[2] A. ODGAARD,[1] and R. HUISKES[2]

[1]*Orthopaedic Research Laboratory, Department of Orthopaedic Surgery, Aarhus University Hospital, Aarhus, Denmark*
[2]*Orthopaedic Research Laboratory, Institute of Orthopaedics, University of Nijmegen, Nijmegen, The Netherlands*

The hypothesis that trabecular morphology can predict the elastic properties of cancellous bone has only partly been verified and no predictive analytical model is currently available. Such models are becoming increasingly relevant as the resolution levels of three-dimensional scanning techniques approach the size of trabeculae. This study took advantage of micro-finite-element methods and tested the aforementioned hypothesis in normal cancellous bone material collected at six anatomical locations from 56 individuals. Numerical analysis was based on high-resolution three-dimensional computer reconstructions of cancellous bone specimens from which the complete elastic characteristics and trabecular morphology, represented by three different fabric measures (the mean intercept length and two volume-based ones), were calculated. Each fabric measure was analyzed individually using the tensorial relationships derived by Cowin (*Mech Mater* 4:137–147; 1985). Models for both stiffness and compliance entries were developed. The models based on stiffness entries could explain 93.4%–95.6% of the variance, whereas those based on compliance entries could explain 89.2%–89.4%. When using the former model, the MIL (mean intercept length measure) performed slightly better than the two volume-based measures, VO (volume orientation) and SVD (star volume distribution), with 23% less remaining variance. The high correlations found strongly support the hypothesis and increase the hope that, on the basis of information on trabecular morphology, it will be possible to obtain considerably better estimates of bone quality in vivo compared with the rough two-dimensional density measurements used today. (Bone 25:481–486; 1999)

Key Words: Bone mechanics; Finite-element analysis; Cancellous bone architecture; Fabric.

Introduction

Knowledge about the mechanical properties of cancellous bone is essential for the determination of bone fracture risk in osteoporosis and other pathological conditions involving impaired bone strength. The direct measurement of bone mechanical properties from compression tests, however, has been shown to yield inaccurate and incomplete results when using excised bone specimens[14,16,17,23] and is impossible in vivo. Consequently, the information needed for patient diagnosis cannot be obtained from direct mechanical tests.

The mechanical properties of cancellous bone are determined by the properties of its bone tissue and its architecture. For this reason, it has been proposed to determine the mechanical properties of bone in an indirect way, based on measurements of its architecture and tissue properties. The mathematical basis for relationships between bone elastic properties, given by nine orthotropic elastic constants, and bone architecture, given by volume fraction and a fabric tensor, is well established by the work of Cowin,[2] who developed a polynomial relationship. In all these relationships a number of constants appear that must be determined by correlating fabric and mechanical parameters measured in experiments. Several earlier studies were conducted to determine these constants, but no accurate and general relationships have as yet been found.

In early studies, only the bone volume fraction (or apparent density) was measured to quantify bone architecture.[1,18,24] In these studies, reasonable correlations between bone density and bone elastic modulus and strength were found. Later studies have included a fabric measure to account for the anisotropy of bone architecture. In most of these studies, relationships were determined by correlating Young's moduli and Poisson ratios, measured from compression tests, with the results of the surface-based mean intercept length (MIL) fabric measure for a large number of cubic bone specimens.[4,7,8,25,27] Relationships found in these studies were generally accurate with squared correlation coefficients of $R^2 > 0.72$, but these were incomplete, because only a subset of the nine orthotropic elastic constants could be predicted. Moreover, the relationships found were not the same in the studies. Part of the unexplained variation may be due to errors in the compression tests, errors in the fabric measurements, and differences in the bone tissue properties. The differences between studies may be due to the differences between specimen groups, indicating that these groups were not representative for bone in general.

Recently, new computer methods have been introduced that, given certain hard tissue properties, allow for the elimination of many of the uncertainties involved with the compression test and the fabric measurements, thus enabling to find the "pure" relationships between architectural and mechanical parameters.[31] With these methods, detailed three-dimensional computer reconstructions of cancellous bone specimens are used for real three-dimensional fabric measurements. After conversion to micromechanical finite-element (μ-FEA) models, these computer models also allow for the calculation of all elastic constants of recon-

Address for correspondence and reprints: Dr. Jesper Kabel, Orthopaedic Research Laboratory, Aarhus University Hospital, Nørrebrogade 44-1A, DK-8000 Aarhus C, Denmark. E-mail: jesper@biomeklab.aau.dk

8756-3282/99/$20.00
PII S8756-3282(99)00190-8

(equation 3), as used by others,[27,31] can be developed. Both types of relationships were analyzed to test which model gave the best prediction of elastic variables. The relationships were normalized to the tissue modulus to obtain generally applicable results. These included relationships based on stiffness coefficients:

$$c_{iiii} = E_t[k_1 + 2k_6 + (k_2 + 2k_7)II + 2(k_3 + 2k_8)\lambda_i + (2k_4 + k_5 + 4k_9)\lambda_i^2]$$

$$c_{iijj} = E_t[k_1 + k_2 II + k_3(\lambda_i + \lambda_j) + k_4(\lambda_i^2 + \lambda_j^2) + k_5\lambda_i\lambda_j]$$

$$c_{ijij} = E_t[k_6 + k_7 II + k_8(\lambda_i + \lambda_j) + k_9(\lambda_i^2 + \lambda_j^2)] \quad (2)$$

and relationships based on compliance coefficients:

$$s_{iiii} = \frac{1}{E_i} = \frac{1}{E_t}[k'_1 + 2k'_6 + (k'_2 + 2k'_7)II + 2(k'_3 + 2k'_8)\lambda_i + (2k'_4 + k'_5 + 4k'_9)\lambda_i^2]$$

$$s_{iijj} = \frac{-\nu_{ij}}{E_i} = \frac{-\nu_{ji}}{E_j} = \frac{1}{E_t}[k'_1 + k'_2 II + k'_3(\lambda_i + \lambda_j) + k'_4(\lambda_i^2 + \lambda_j^2) + k'_5\lambda_i\lambda_j]$$

$$s_{ijij} = \frac{1}{G_{ij}} = \frac{4}{E_t}[k'_6 + k'_7 II + k'_8(\lambda_i + \lambda_j) + k'_9(\lambda_i^2 + \lambda_j^2)] \quad (3)$$

where $i, j = 1, 2, 3$; $i \neq j$ and $II = \lambda_1\lambda_2 + \lambda_1\lambda_3 + \lambda_2\lambda_3$.

In these relationships, nine functions of apparent density or volume fraction appear (equations 4 and 5), which must be calculated such that the best fit between fabric and elastic variables can be obtained. In agreement with earlier studies,[27,31] the functions of density were chosen as power functions with two constants (k_{ma} and k_{mb}) per function, in total 18, but the analysis was extended to allow the power of volume fraction to vary as well in an interval (0.5–3.0), as other workers have found stiffness and strength to be dependent on bone density by a power factor within this interval[15]:

$$k_m(V_V) = k_{ma} + k_{mb}V_V^p \text{ where } m = 1, 2, \ldots, 9 \text{ and } p \in [0.5; 3.0] \quad (4)$$

and:

$$k'_m(V_V) = k'_{ma} + k'_{mb}V_V^p \text{ where } m = 1, 2, \ldots, 9 \text{ and } p \in [0.5; 3.0] \quad (5)$$

For the analysis the elastic data were sorted such that $E_1 > E_2 > E_3$, and the fabric eigenvalues were sorted correspondingly, $\lambda_1 > \lambda_2 > \lambda_3$. Relationships for each fabric measure were calculated by performing a joint fit to the relationships (equations 2 and 3) using singular value decomposition.[26] The goodness of each fit was evaluated by correlating elastic coefficients obtained from finite element analysis to elastic coefficients predicted from the models. An adjusted squared correlation coefficient (R^2_{adj}), developed by Turner et al.,[27] was used as a goodness-of-fit criterion:

$$R^2_{adj} = 1 - (1 - R^2)(N - 1)/(N - K - 1) \quad (6)$$

with N the number of observations and K the number (= 19) of variables. Using the same set of constants as for the joint fit, the goodness of fit for the individual compliance and stiffness matrix entries as well as technical constants (E_i, G_i, and ν_{ij}) were calculated for comparison with the results of earlier studies.[27,31]

Table 2. Descriptive statistics of the combined series of data

Variable	Mean	SD	Skewness	Range
V_V	0.16	0.08	0.6	0.03–0.35
E_i	39.2	38.8	1.6	1.41–196
G_{ij}	12.6	12.1	1.7	0.38–67.9
ν_{ij}	0.21	0.12	0.7	0.02–0.73
c_{ijkl}	21.8	30.2	3.0	0.28–216
s_{ijkl}	0.09	0.20	5.1	−0.13–2.62

E_i is Young's moduli, G_{ij} is shear moduli, and ν_{ij} is Poisson ratio. c_{ijkl} and s_{ijkl} are the stiffness and compliance entries, respectively. Note that the values of E_i, G_{ij}, c_{ijkl}, and s_{ijkl} are normalized to tissue modulus.

To determine if a possible correlation was due to a dominant effect from one of the data series only, the predictive power was tested for each series separately using relationships that turned out to be the best case for the pooled data.

Results

The volume fractions represented by the combined series covered a range from 3% to 35% (mean 16%, SD 8%) (**Table 2**). The Young's moduli (E_i) ranged from 1.4 to 196 and the shear moduli (G_{ij}) ranged from 0.38 to 68, both normalized to tissue modulus. The Poisson ratios covered a range from 0.02 to 0.73.

For all relationships a well-defined maximum of R^2_{adj} was found for the joint fit when the power factor of volume fraction was varied in the interval from 0.5 to 3. The relationships based on the stiffness entries (equation 2) showed the best correlations; that is, the highest R^2_{adj} values for the correlation of predicted to calculated elastic variables in the relationships (equations 2 and 3). For these relationships the three fabric measurements and volume fraction explained between 93.9% and 95.6% of the variation of the stiffness entries, whereas, for the other relationships based on compliance entries, 89.2%–89.4% of the variation of the compliance entries was explained (**Table 3**).

The best fit was found for the relationships based on stiffness entries (Table 3) and, for such relationships, the MIL fabric measure was a better predictor than both the VO and SVD measures as it decreased the remaining variance by approximately 23% (from 5.7% found for VO to 4.4%). Looking at the technical constants only, the relationships based on the stiffness entries could predict these quantities and only the Young's moduli and the shear moduli could be predicted (Table 3). For the Poisson ratios, nonsignificant or very weak correlations ($R^2_{adj} < 0.08$) were found.

As the relationships based on stiffness entries and MIL were the best performing, the predictive power of this model was evaluated for each series separately (**Table 4**). The model could explain 96.5% of the variation in series 1 and 95.4% in series 2, suggesting that both series contributed almost equally to the correlation of the pooled data.

The 18 constants (k_{ma} and k_{mb}) corresponding to the best fit (i.e., largest R^2_{adj}) calculated for each fabric measure are listed in **Table 5**. Inserting the constants for the best case (MIL measure and relationships based on stiffness entries, equation 2) the relationships can be written as:

$$c_{iiii} = E_t[2.91 \cdot 10^{-2} + 0.133II - 0.511\lambda_i + 0.821\lambda_i^2] + E_t[0.865 - 5.50II + 5.14\lambda_i - 7.54 \cdot 10^{-2}\lambda_i^2]V_V^{1.6}$$

$$c_{iijj} = E_t[-6.52 \cdot 10^{-3} + 0.276II - 0.263(\lambda_i + \lambda_j) + 0.263(\lambda_i^2 + \lambda_j^2) + 0.274\lambda_i\lambda_j] + E_t[0.624 + 11.6II - 13.4(\lambda_i + \lambda_j) + 11.6(\lambda_i^2 + \lambda_j^2) + 18.8\lambda_i\lambda_j]V_V^{1.6}$$

JTTEE5
DOI: 10.1007/s11666-009-9344-z
1059-9630/$19.00 © ASM International

Elastic and Conductive Properties of Plasma-Sprayed Ceramic Coatings in Relation to Their Microstructure: An Overview

Example where tensors are needed

Igor Sevostianov and Mark Kachanov

(Submitted February 2, 2009; in revised form April 17, 2009)

This article focuses on micromechanics-based models that explicitly express the elastic and conductive properties of plasma-sprayed ceramic coatings in terms of relevant microstructural parameters. These parameters reflect, in an integral way, the density and the orientation distribution of microcracks; they apply to strongly oblate pores as well. On the other hand, the porosity parameter usually plays a secondary role. Partial contacts between crack faces—a factor of major importance—are reflected via appropriate reduction of crack densities. The effect of various "irregularities" of crack shapes is discussed. Case studies of YSZ coatings demonstrate how the micromechanics-based modeling can be used and directly interfaced with 2-D image data.

Keywords coating, conductivity, cross-property, elasticity, plasma sprayed

1. Introduction

The present review discusses the elastic stiffness of plasma-sprayed ceramic coatings and their thermal conductivity in relation to their microstructure. We focus on explicit relations between the said properties and relevant microstructural features.

Plasma-sprayed ceramic coatings have a lamellar microstructure consisting of elongated, flat-like splats of diameters between 100 and 200 μm and thicknesses between 2 and 10 μm, formed by a rapid solidification (Fig. 1a). The porous space comprises "irregular" mixture of cracks and pores of diverse shapes (Fig. 1b). Their orientation distribution is usually nonrandom (with tendency to be either parallel or normal to the substrate) resulting in noticeable anisotropy. The problem arises of their proper quantitative characterization, i.e., of identification of the *argument* of the function

$$\text{effective property} = f\left(\underbrace{\text{microstructural parameter}}_{?}\right) \qquad \text{(Eq 1.1)}$$

prior to discussing possible forms of this function.

Igor Sevostianov, Department of Mechanical Engineering, New Mexico State University, PO Box 30001, Las Cruces, NM 88003; and **Mark Kachanov**, Department of Mechanical Engineering, Tufts University, Medford, MA 02155. Contact e-mails: igor@nmsu.edu and mark.kachanov@tufts.edu.

The basic requirement to the proper parameter is that it must represent individual defects according to their actual contributions to the considered property. For example, crack density parameter takes the individual crack contributions proportionally to crack sizes cubed, since this corresponds to their contributions to the effective compliance and to the conductivity.

Violation of this basic requirement may lead to inconsistencies. For illustration, we consider a family of strongly oblate pores. Their contributions to the effective compliance are almost independent of their aspect ratios, as long as they are below 0.1 (see the discussion in Sect 2). Let us assume that we express the effective compliance in terms of volume fraction of the pores (porosity P). Then, if the aspect ratios are changed, say, from 0.05 to 0.1 this would increase P by a factor of two, but the effective compliance will remain almost unchanged. If, on the other hand, we increase the number of pores by a factor of two and reduce their aspect ratios by the same factor, P will remain the same, but pore compliances will increase several times. In other words, the function (1.1) will not be single valued, if its argument is P. If, however, we recognize that strongly oblate pores are almost identical to cracks in their effect on the linear elastic properties, and identify crack density as the proper argument of (1.1), these difficulties are not encountered.

For complex microstructures, the identification of such parameters is a challenging problem. In the general context of materials science, this problem was reviewed in Ref 1.

Quantitative characterization of microstructures—i.e., identification of the proper microstructural parameters—depends on the physical property considered. For example, parameters that control the elastic and the conductive properties are largely similar, but, in cases of overall anisotropy, they are not identical. Further, if the conductivity of the gas filling the pores is to be taken into

Published online: 27 June 2009

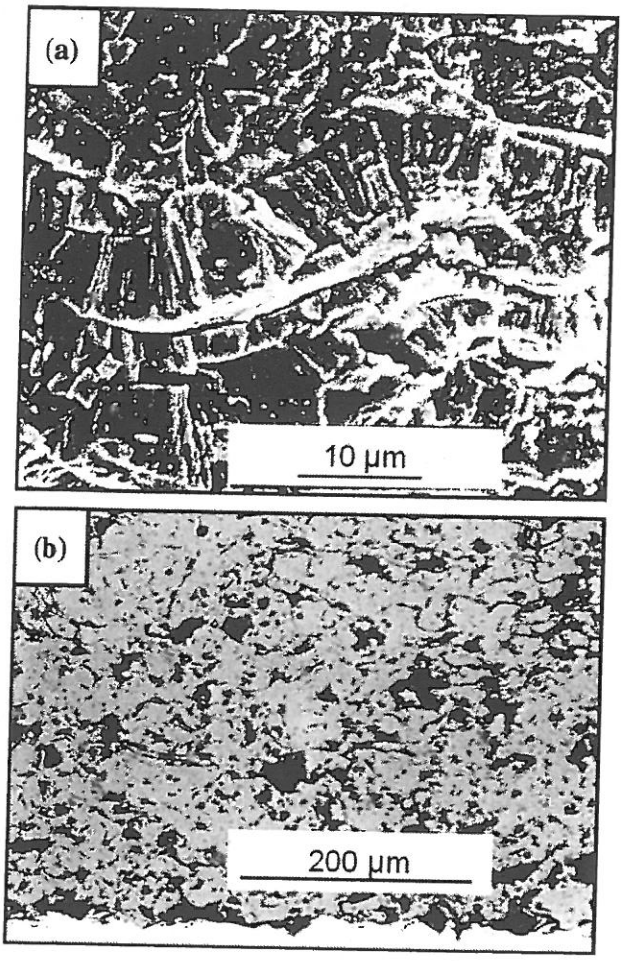

Fig. 1 Typical microstructure of plasma-sprayed ceramic coatings at different magnifications

account, the crack opening—albeit small—may become important, and this would require modification of the microstructural parameter. Importantly, the microstructural parameters that control the permeability, or fracture, may be entirely different from the ones relevant to the elastic/conductive properties.

We focus on the three-dimensional modeling. As far as 2-D models and computations are concerned, they are of qualitative and illustrative—but not quantitative—value. For example, the compliance/conductivity contributions of cracks and pores scale as their sizes *cubed* in 3-D, but *squared* in 2-D, and this difference is of major consequence for mixtures of defects of diverse sizes.

Remark We consider the *linear* elastic effective properties. This may present a limitation in the case of narrow, crack-like pores in the field of compressive stresses: if the latter are high enough to close some of the pores, the response is nonlinear (we refer to the review, Ref 2, for a discussion of nonlinear effects). Yet another limitation concerning conductivity is that cracks and pores are treated as ideal insulators, neglecting heat transfer across them, due to radiation or conductivity of the gas.

Three different approaches to modeling of microstructure of plasma-sprayed coatings have been suggested in literature:

A. Treating *contacts* between splats (that alternate with much larger no-contact zones) as dominant elements of the microstructure; the effective properties are then controlled by appropriate contact characteristics. Such modeling was developed in the context of conductivity (Ref 3); it was refined and extended to the elastic properties in a number of subsequent works; for their overview, we refer to Ref 4. One limitation of these models is that the contacts were considered as non-interacting ones, whereas interactions between contacts are generally strong and have substantial effect on the overall properties (Ref 5). We also mention that the assumption of smallness of contact areas may or may not correspond to the coating microstructure; for example, the data in Ref 6 show that contact areas may be comparable to no-contact ones. Yet another limitation concerns anisotropy: a full set of anisotropic effective constants was not given in the mentioned works. An important observation is that the cross-property connections discussed in Sect 4 imply that models for the conductive and the elastic properties should be compatible. Such compatibility is not always clear in models of this kind (see Ref 4).

B. Treating *pores and microcrack*s as dominant features of the microstructure; parameters of their concentration are then the controlling microstructural parameters. In Ref 7 and 8, it is suggested to represent the porous space by two families of oblate pores, of perfectly vertical and perfectly horizontal orientations; a similar model was developed in Ref 9. One shortcoming of these models is that the effective elastic constants were expressed in terms of *volume fractions* of the two families (rather than crack densities). This leads to difficulties discussed above, and translates into very high sensitivity of the effective constants to the exact values of aspect ratios—a parameter that in addition to being unimportant may not be known. In addition, it is unclear how to *define* aspect ratios for pores of irregular shapes. In Ref 10, two families of microcracks—perfectly vertical and perfectly horizontal, plus spherical pores—were treated as the main microstructural elements, and the effective elastic constants were expressed in terms of crack density and porosity. The latter model did not consider the orientation scatter (that is, typically, substantial); this factor was accounted for in Ref 11-13.

The above-mentioned works did not take into account the presence of partial contacts between crack faces—the factor of major importance producing very strong effect on the elastic and conductive properties. This limitation

without the β-term omitted are quite close and are within typical error margins involved in processing image data and measuring the effective constants. Hence the β-term can, typically, be neglected and cracks can be characterized solely by the crack density tensor α.

The characterization of cracks solely by the crack density tensor α leads to a drastically reduced number of independent elastic constants—from nine, in the general case of orthotropy, to *only four*, if the orthotropy is due to cracks (regardless of their orientation distribution): all the constants can be expressed in terms of three Young's moduli, E_1, E_2, E_3, and one constant of the bulk material ν_0/E_0. In the case of transverse isotropy relevant to the coatings (x_3 is the symmetry axis), $E_1 = E_2$ and the number of independent effective constants is reduced to *only three*. In this case, the constants are given in terms of crack density components $\alpha_{11} = \alpha_{22}$ and α_{33} as follows:

$$E_1 = E_2 = E_0\left[1+\frac{32(1-\nu_0^2)}{3(2-\nu_0)}\alpha_{11}\right]^{-1},$$

$$E_3 = E_0\left[1+\frac{32(1-\nu_0^2)}{3(2-\nu_0)}\alpha_{33}\right]^{-1}$$

$$G_{12} = G_0\left[1+\frac{32(1-\nu_0)}{3(2-\nu_0)}\alpha_{11}\right]^{-1}, \qquad \text{(Eq 3.2)}$$

$$G_{13} = G_{23} = G_0\left[1+\frac{16(1-\nu_0)}{3(2-\nu_0)}(\alpha_{11}+\alpha_{33})\right]^{-1}$$

$$\frac{\nu_{12}}{E_1} = \frac{\nu_{31}}{E_3} = \frac{\nu_0}{E_0}$$

Reduction of the number of independent constants to only three is expressed in the following relations showing that the shear moduli are not independent constants:

$$\frac{1}{G_{12}} = \frac{1}{E_1}+\frac{1}{E_2}+\frac{2\nu_0}{E_0}, \quad \frac{1}{G_{13}} = \frac{1}{E_1}+\frac{1}{E_3}+\frac{2\nu_0}{E_0} \qquad \text{(Eq 3.3)}$$

For the specific transversely isotropic orientation distribution given by (2.6), components α_{11} and α_{33} are given in terms of crack densities of the horizontal and vertical families, ρ_h and ρ_v and their scatter parameters, λ_h and λ_v by formulas (2.7).

We now modify the expression (3.1) to account for the porosity effect according to the Mori-Tanaka's scheme (MTS) where defects are placed into the average stress, over the solid phase. The average stress increases by a factor of $(1-p)^{-1}$, which enters, therefore, as a multiplier at the compliances given by (3.1). There are two sources of porosity—due to pores (denoted by p_p) and due to slightly open cracks (denoted by p_c); the total porosity $p = p_p + p_c$. Hence the MTS modification involves two factors:

- The effect of pores that is be added to the effect of cracks in the framework of NIA, by assuming that pores are placed in the externally applied stress unperturbed by neighbors;
- The amplification effect due to the elevated average stress in the solid matrix; it is described by the amplifying factor $(1-p)^{-1}$ applied to both pores and cracks.

Remark Although slight openings of cracks produce a very minor effect on their compliance contributions (Fig. 3), they affect the overall compliance by contributing to the amplifying factor $(1-p)^{-1}$.

These considerations yield the following modification of (3.1):

$$\Delta S_{ijkl} = \frac{32(1-\nu_0^2)}{3(2-\nu_0)E_0}\frac{1}{1-p} \times \left[\frac{1}{4}(\delta_{ik}\alpha_{jl}+\delta_{il}\alpha_{jk}+\delta_{jk}\alpha_{il}+\delta_{jl}\alpha_{ik})-\frac{\nu_0}{2}\beta_{ijkl}\right] + \frac{3(1-\nu_0)}{2(7-5\nu_0)E_0}\frac{p_p}{1-p} \times \left[5(1+\nu_0)(\delta_{ik}\delta_{jl}+\delta_{il}\delta_{jk})-(1+5\nu_0)\delta_{ij}\delta_{kl}\right] \qquad \text{(Eq 3.4)}$$

where the second term reflects the effect of pores, and the amplifying factor $(1-p)^{-1}$ is applied to both pores and cracks. Applying this formula to the orientation distribution (2.6) we obtain the following modification of formulas (3.2):

$$E_1 = E_2 = E_0\left[1+\frac{32(1-\nu_0^2)}{3(2-\nu_0)}\frac{\alpha_{11}}{1-p}+\frac{3(1-\nu_0)(9+5\nu_0)}{2(7-5\nu_0)}\frac{p_p}{1-p}\right]^{-1}$$

$$E_3 = E_0\left[1+\frac{32(1-\nu_0^2)}{3(2-\nu_0)}\frac{\alpha_{33}}{1-p}+\frac{3(1-\nu_0)(9+5\nu_0)}{2(7-5\nu_0)}\frac{p_p}{1-p}\right]^{-1}$$

$$G_{12} = G_0\left[1+\frac{32(1-\nu_0)}{3(2-\nu_0)}\frac{\alpha_{11}}{1-p}+\frac{15(1-\nu_0)}{(7-5\nu_0)}\frac{p_p}{1-p}\right]^{-1}$$

$$G_{13} = G_{23} = G_0\left[1+\frac{16(1-\nu_0)}{3(2-\nu_0)}\frac{\alpha_{11}+\alpha_{33}}{1-p}+\frac{15(1-\nu_0)}{(7-5\nu_0)}\frac{p_p}{1-p}\right]^{-1}$$

$$\frac{\nu_{12}}{E_1} = \frac{\nu_{31}}{E_3} = \frac{\nu_0}{E_0}\left[1+\frac{3(1-\nu_0)(1+5\nu_0)}{2\nu_0(7-5\nu_0)}\frac{p_p}{1-p}\right] \qquad \text{(Eq 3.5)}$$

4. The Conductive Properties and the Cross-Property Connection

For the effective conductive properties, quantitative characterization of the microstructure is similar—although not identical—to the one for the elastic properties. The key quantity is the resistivity contribution of a defect; the extra resistivity of a representative volume V due to multiple defects is a sum of the individual contributions. In analogy to formulas (2.1) for the elastic compliances, we compare the resistivity contribution Δr of the circular crack of radius a placed in a uniform field of heat flux in the direction x_1 normal to the crack and that of the

Vectors

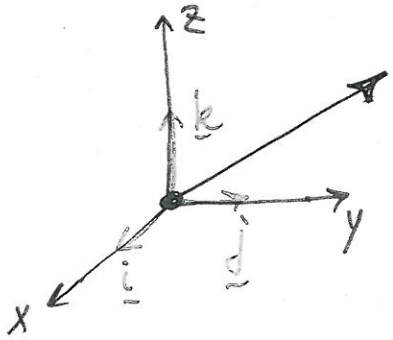

$$\underset{\sim}{a} = a_x \underline{i} + a_y \underline{j} + a_z \underline{k}$$

↑ component representation in a chosen coord. syst.

↑ objective (indep. of coord. system) physical quantity, like force, velocity

Switch to different notations:

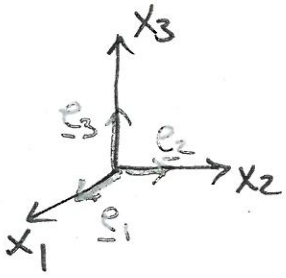

base vectors $\underset{\sim}{e}_1$, $\underset{\sim}{e}_2$, $\underset{\sim}{e}_3$:

- are orthogonal
- have unit length

$$\underline{e}_i \cdot \underline{e}_j = \begin{cases} 1 & \text{if } i=j \\ 0 & \text{if } i \neq j \end{cases} = \delta_{ij}$$ (Kronecker's delta)

Indicial notation for summation:

$$\underset{\sim}{a} = \sum_i a_i \underset{\sim}{e}_i = a_i \underset{\sim}{e}_i$$ - repeated index ⇒ summation

$$\underset{\sim}{a} \cdot \underline{b} = a_i \underset{\sim}{e}_i \cdot b_j \underset{\sim}{e}_j = a_i b_j \delta_{ij} = a_i b_i$$

Tensors : vector f-ns of vector argument

$$\underset{\sim}{T} : \underset{\sim}{u} \to \underset{\sim}{v}$$

(in case $\underset{\sim}{u}, \underset{\sim}{v}$ are position vectors this is transform. of space

that is linear : $v_i = T_{ij} u_j$ (3 eq-ns, $i = 1, 2, 3$)

Matrix T_{ij} represents $\underset{\sim}{T}$ in a chosen coord. system

write in the form

$$\underset{\sim}{v} = \underset{\sim}{T} \cdot \underset{\sim}{u}$$

Example : mirror reflection about a plane

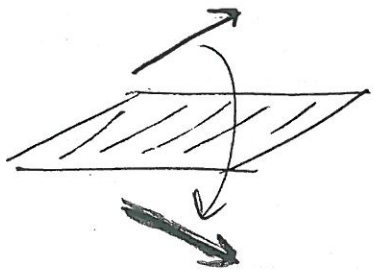

$\Rightarrow$ in coord. system

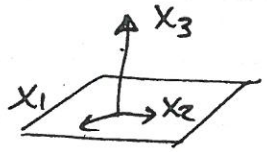

$$T_{ij} = \begin{vmatrix} 1 & 0 & 0 \\ 0 & 1 & 0 \\ 0 & 0 & -1 \end{vmatrix}$$

Indeed:

$$v_1 = T_{1j} u_j = T_{11} u_1 = u_1$$

$$v_2 = T_{2j} u_j = T_{22} u_2 = u_2$$

$$v_3 = T_{3j} u_j = T_{33} u_3 = -u_3$$

Special Tensor – Dyad

Take two vectors $\underset{\sim}{a}$, $\underset{\sim}{b}$. Define the following transformation $\underset{\sim}{u} \to \underset{\sim}{v}$:

$$\underset{\sim}{v} = \underset{\sim}{a}(\underset{\sim}{b}\cdot\underset{\sim}{u})$$

$$= \underset{\sim}{a}\,(b_j u_j) \quad \text{parentheses can be dropped} \quad = \underset{\sim}{a} b_j u_j$$

Or

$$v_i = \underbrace{a_i b_j}\, u_j$$

T_{ij} – components of tensor $\underset{\sim}{a}\underset{\sim}{b}$

$\underset{\sim}{u}$ is transformed into a vector $\underset{\sim}{v}$ that:

- has length $|\underset{\sim}{a}|\, \underset{\sim}{b}\cdot\underset{\sim}{u}$
- has direction of $\underset{\sim}{a}$

Special dyads: take $\underset{\sim}{a}$ and $\underset{\sim}{b}$ as base unit vectors

for example, $\underset{\sim}{e}_1\underset{\sim}{e}_1$, $\underset{\sim}{e}_2\underset{\sim}{e}_3$, ---

$$\underset{\sim}{v} = \underset{\sim}{e}_1\underset{\sim}{e}_3\cdot\underset{\sim}{u} = u_3\underset{\sim}{e}_1$$

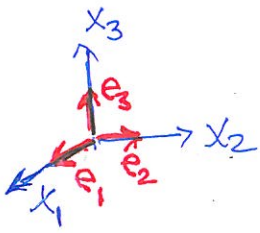

Any vector: a sum of base vectors

$$\underset{\sim}{a} = a_i \underset{\sim}{e}_i$$

a_i: components; $\underset{\sim}{e}_i$: base vectors

Similarly, any tensor is a sum of base dyads:

$$\underline{T} = T_{ij}\, \underset{\sim}{e}_i \underset{\sim}{e}_j$$

T_{ij}: components in this coord. system; $\underset{\sim}{e}_i \underset{\sim}{e}_j$: base dyads

To find matrix T_{ij} of $\underline{T}$ in a chosen coord. system:
watch: what $\underline{T}$ does to base vectors

$$\underline{T} \cdot \underset{\sim}{e}_1 = T_{ij}\, \underset{\sim}{e}_i\, \underbrace{\underset{\sim}{e}_j \cdot \underset{\sim}{e}_1}_{\delta_{j1}} = T_{i1}\, \underset{\sim}{e}_i$$

$$\underline{T} \cdot \underset{\sim}{e}_2 = T_{i2}\, \underset{\sim}{e}_i$$

$$\underline{T} \cdot \underset{\sim}{e}_3 = T_{i3}\, \underset{\sim}{e}_i$$

T_{i1}: 1st column of T_{ij}

Example Mirror reflection about plane

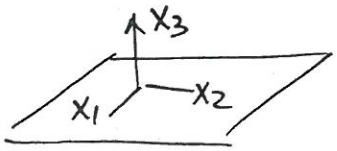

← In this coord. system:

$$\underline{T} \cdot \underset{\sim}{e}_1 = \underset{\sim}{e}_1 = 1 \cdot \underset{\sim}{e}_1 + 0 \cdot \underset{\sim}{e}_2 + 0 \cdot \underset{\sim}{e}_3$$

$$\Rightarrow \underline{T} = \underset{\sim}{e}_1 \underset{\sim}{e}_1 + \underset{\sim}{e}_2 \underset{\sim}{e}_2 - \underset{\sim}{e}_3 \underset{\sim}{e}_3 \quad \text{- dyadic represent.}$$

$$\Rightarrow T_{ij} = \begin{vmatrix} 1 & 0 & 0 \\ 0 & 1 & 0 \\ 0 & 0 & -1 \end{vmatrix}$$

Convenience: Apply to any vector: $\underline{T} \cdot (3\underset{\sim}{e}_1 + 2\underset{\sim}{e}_2 + 4\underset{\sim}{e}_3) = 3\underset{\sim}{e}_1 + 2\underset{\sim}{e}_2 - 4\underset{\sim}{e}_3$ ← as expected

Example 2 — 90° rotation about axis

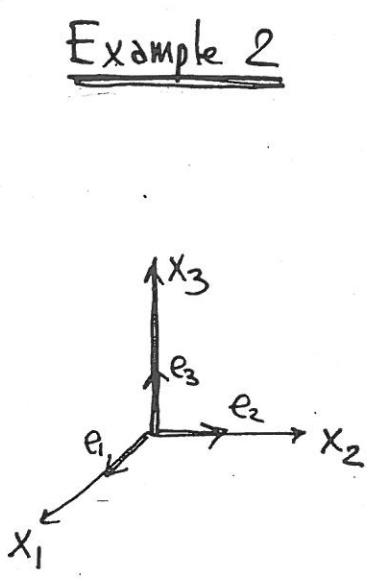

Choosing this axis as X_3 :

$$\underset{\sim}{T} \cdot \underline{e}_1 = \underline{e}_2 \Rightarrow \begin{pmatrix} 0 \\ 1 \\ 0 \end{pmatrix}$$

$$\underset{\sim}{T} \cdot \underline{e}_2 = -\underline{e}_1 \Rightarrow \begin{pmatrix} -1 \\ 0 \\ 0 \end{pmatrix}$$

$$\underset{\sim}{T} \cdot \underline{e}_3 = \underline{e}_3 \Rightarrow \begin{pmatrix} 0 \\ 0 \\ 1 \end{pmatrix}$$

$$\Rightarrow \begin{vmatrix} 0 & -1 & 0 \\ 1 & 0 & 0 \\ 0 & 0 & 1 \end{vmatrix}$$

$$\Rightarrow \quad \underset{\sim}{T} = -\underline{e}_1 \underline{e}_2 + \underline{e}_2 \underline{e}_1 + \underline{e}_3 \underline{e}_3$$

Convenience : can find now:
what happens with any vector:

$$\underset{\sim}{T} \cdot (3\underline{e}_1 - \underline{e}_2 + 7\underline{e}_3) = 3\underline{e}_2 + \underline{e}_1 + 7\underline{e}_3$$

↑ no change as expected

Two Successive Rotations

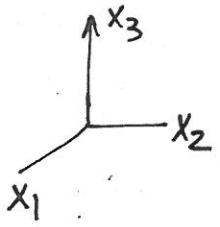

(A) 90° about x_3 counterclockwise

followed by

(B) α-angle, clockwise about x_2

As found earlier, for (A) we have : $\underset{\sim}{T}^{(A)} = -\underline{e}_1\underline{e}_2 + \underline{e}_2\underline{e}_1 + \underline{e}_3\underline{e}_3$

$$T_{ij} = \begin{vmatrix} 0 & -1 & 0 \\ 1 & 0 & 0 \\ 0 & 0 & 1 \end{vmatrix}$$

For (B) :

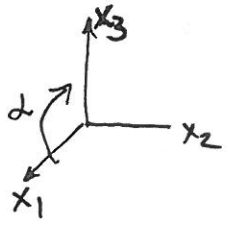

first column

$\underset{\sim}{T}^{(B)} \cdot \underline{e}_1 = \cos\alpha\, \underline{e}_1 + \sin\alpha\, \underline{e}_3 \rightarrow (\cos\alpha,\ 0,\ \sin\alpha)$

$\underset{\sim}{T}^{(B)} \cdot \underline{e}_2 = \underline{e}_2 \rightarrow (0,\ 1,\ 0)$

$\underset{\sim}{T}^{(B)} \cdot \underline{e}_3 = -\sin\alpha\, \underline{e}_1 + \cos\alpha\, \underline{e}_3 \rightarrow (-\sin\alpha,\ 0,\ \cos\alpha$

$$\underset{\sim}{T}^{(B)} = \begin{pmatrix} \cos\alpha & 0 & -\sin\alpha \\ 0 & 1 & 0 \\ \sin\alpha & 0 & \cos\alpha \end{pmatrix} = \cos\alpha\, \underline{e}_1\underline{e}_1 - \sin\alpha\, \underline{e}_1\underline{e}_3 + \underline{e}_2\underline{e}_2 + \sin\alpha\, \underline{e}_3\underline{e}_1 + \cos\alpha\, \underline{e}_3\underline{e}_3$$

Overall transformation : $\underset{\sim}{T}^B \cdot \underset{\sim}{T}^A = -\cos\alpha\, \underline{e}_1\underline{e}_2 - \sin\alpha\, \underline{e}_3\underline{e}_2 + \underline{e}_2\underline{e}_1 - \sin\alpha\, \underline{e}_1\underline{e}_3 + \cos\alpha\, \underline{e}_3\underline{e}_3$

or

$$\begin{pmatrix} 0 & -\cos\alpha & -\sin\alpha \\ 1 & 0 & 0 \\ 0 & -\sin\alpha & \cos\alpha \end{pmatrix}$$

Note : can easily find now what $\underset{\sim}{T}^B \cdot \underset{\sim}{T}^A$ does to any $\underset{\sim}{u}$

Note: Result of two successive transformations depends on the order!

Example:

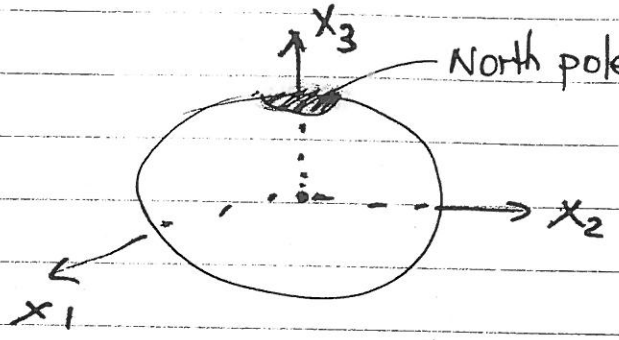

(1) Rot. 90° about x_3

(2) - — — - x_1

> and interchange

Summary : tensor $\underline{\underline{T}}$ is a transformation of the for

$$\underset{\sim}{v} = \underline{\underline{T}} \cdot \underset{\sim}{u}$$

in components:

$$v_i = T_{ij} u_j$$

In dyadic form:

$$\underset{\sim}{v} = \underline{\underline{T}} \cdot \underset{\sim}{u}$$

$T_{ij} \underline{e}_i \underline{e}_j$ $\qquad$ $u_k \underline{e}_k$

δ_{jk}

$$= T_{ij} u_j \underset{\sim}{e}_i = \underset{\sim}{v}$$

$$= \underbrace{T_{ij} u_j}_{v_i} \underset{\sim}{e}_i$$

Unit tensor (identity transformation): leaves everything in its place

$$\underset{\sim}{I} \cdot \underset{\sim}{e}_1 = \underset{\sim}{e}_1 \quad , \text{ etc}$$

$$I_{ij} = \begin{pmatrix} 1 & & \\ & 1 & 0 \\ 0 & & 1 \end{pmatrix}$$

or $$\underset{\sim}{I} = \underset{\sim}{e}_1 \underset{\sim}{e}_1 + \underset{\sim}{e}_2 \underset{\sim}{e}_2 + \underset{\sim}{e}_3 \underset{\sim}{e}_3$$

$$= \delta_{ij} \underset{\sim}{e}_i \underset{\sim}{e}_j = \underset{\sim}{e}_i \underset{\sim}{e}_i$$

Apply to any vector $\underset{\sim}{u}$:

$$\underset{\sim}{I} \cdot \underset{\sim}{u} = \delta_{ij} \underset{\sim}{e}_i \underset{\sim}{e}_j \cdot u_k \underset{\sim}{e}_k$$

δ_{jk}

$\delta_{jk} u_k = u_j$

$$= \delta_{ij} u_j \underset{\sim}{e}_i = u_i \underset{\sim}{e}_i = \underset{\sim}{u}$$

Projection tensor:

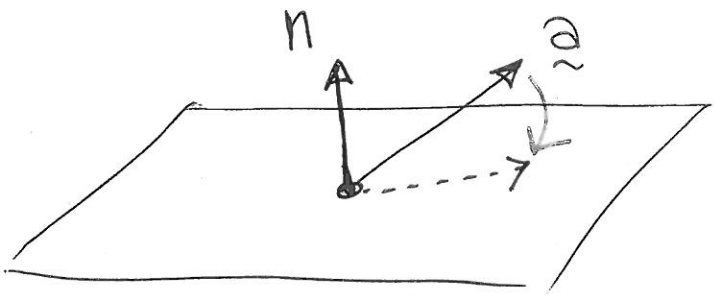

Projects $\underset{\sim}{a}$ on plane (having unit normal n

Projection tensor $\underset{\sim}{P} = \underset{\sim}{I} - \underset{\sim}{n}\underset{\sim}{n}$

Being applied to vector a:

$$\underset{\sim}{P} \cdot \underset{\sim}{a} = \underset{\sim}{a} - (\underset{\sim}{a} \cdot \underset{\sim}{n})\,\underset{\sim}{n}$$

- projected vector $\underset{\sim}{a}'$

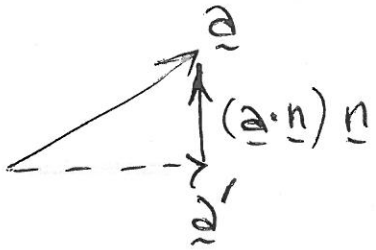

Symmetric Tensor: its matrix of components is symmetric

$$T_{ij} = T_{ji}$$

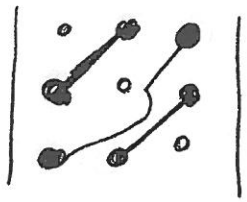

6 independent components

Example: unit tensor I $\begin{pmatrix} 1 & 0 & \\ 0 & 1 & 0 \\ & 0 & 1 \end{pmatrix}$

Antisymm. Tensor: $T_{ij} = -T_{ji}$

If $i=j$ (diagonal comp.): $T_{11} = T_{22} = T_{33} = 0$

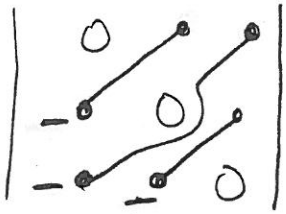

3 independent components

Arbitrary $T_{ij} = \underbrace{\frac{1}{2}(T_{ij} + T_{ji})}_{\text{sym}} + \underbrace{\frac{1}{2}(T_{ij} - T_{ji})}_{\text{antisym}}$

$$\begin{pmatrix} 5 & 3 & 1 \\ 2 & 7 & 0 \\ 1 & 4 & 1 \end{pmatrix} = \begin{pmatrix} 5 & 2.5 & 1 \\ 2.5 & 7 & 2 \\ 1 & 2 & 1 \end{pmatrix} + \begin{pmatrix} 0 & .5 & 0 \\ -.5 & 0 & -2 \\ 0 & 2 & 0 \end{pmatrix}$$

If matrix of components of $\mathbf{T}$ is $\begin{matrix}\text{symm} \\ \text{antisymm}\end{matrix}$ in one coord system

then it is $\begin{matrix}\text{symm} \\ \text{antisymm}\end{matrix}$ in any other system